# Combining COMSOL Modeling with Acoustic Pressure Maps to Design Sono-reactors

*Zongsu Wei and Linda K. Weavers**

Department of Civil, Environmental and Geodetic Engineering

The Ohio State University, Columbus, Ohio, U.S.A 43210

**Corresponding author*

Phone: (614) 292-4061; Fax: (614) 292-3780; E-mail address: weavers.1@osu.edu; Address: The Ohio State University, Department of Civil, Environmental & Geodetic Engineering, 470 Hitchcock Hall, 2070 Neil Avenue, Columbus, OH 43210, USA

## Abstract

Scaled-up and economically viable sonochemical systems are critical for increased use of ultrasound in environmental and chemical processing applications. In this study, computational simulations and acoustic pressure maps were used to design a larger-scale sono-reactor containing a multi-stepped ultrasonic horn. Simulations in COMSOL Multiphysics showed ultrasonic waves emitted from the horn neck and tip, generating multiple regions of high acoustic pressure. The volume of these regions surrounding the horn neck were larger compared with those below the horn tip. The simulated acoustic field was verified by acoustic pressure contour maps generated from hydrophone measurements in a plexiglass box filled with water. These acoustic pressure contour maps revealed an asymmetric and discrete distribution of acoustic pressure due to acoustic cavitation, wave interaction, and water movement by ultrasonic irradiation. The acoustic pressure contour maps were consistent with simulation results in terms of the effective scale of cavitation zones (~10 cm and < 5 cm above and below horn tip, respectively). With the mapped acoustic field and identified cavitation location, a cylindrically-shaped sono-reactor with a conical bottom was designed to evaluate the treatment capacity (~5 L) for the multi-stepped horn using COMSOL simulations. In this study, verification of simulation results with experiments demonstrates that coupling of COMSOL simulations with hydrophone measurements is a simple, effective and reliable scientific method to evaluate reactor designs of ultrasonic systems.

**Keywords:** ultrasound, COMSOL Multiphysics, hydrophone, acoustic field, cavitation

**Nomenclature**

| | |
|---|---|
| $a_n$ | normal acceleration of solid horn (m $s^{-2}$) |
| $A_i$ | amplitude in radius change for $i^{th}$ harmonic |
| c | speed of ultrasound propagation in the water (m $s^{-1}$) |
| $c_E$ | elastic coefficients (6 × 6 matrix; Pa) at constant electric field strength |
| d | piezoelectric strain constant (3 × 6 matrix; m $V^{-1}$) |
| $d^t$ | transposed piezoelectric strain constant matrix (6 × 3; m $V^{-1}$) |
| **D** | electric flux density vector (3 × 1 matrix; C $m^{-2}$) |
| e | dielectric permittivity (3 × 6 matrix; C $m^{-2}$) |
| $e^{i\varphi}$ | alternating current (AC) |
| $e^t$ | transposed dielectric permittivity matrix (6 × 3; C $m^{-2}$) |
| **E** | electric field intensity vector (3 × 1 matrix; V $m^{-1}$) |
| f | frequency of ultrasound (Hz) |
| $f_h$ | bubble oscillation frequency (Hz) |
| $f_R$ | resonance frequency of bubble oscillation (Hz) |
| $\mathbf{F}_V$ | force per volume (N $m^{-3}$) |
| m | integral number |
| n | integral number |
| **n** | unit vector |
| P | acoustic pressure (Pa) |
| $P_A$ | maximum acoustic pressure (Pa) |
| $P_{stat}$ | hydrostatic pressure (Pa) |
| $P_{vapor}$ | vapor pressure (Pa) |

| | |
|---|---|
| $\mathbf{q}$ | dipole source (m $s^{-2}$) |
| R | bubble radius at time t (m) |
| $R_0$ | bubble radius at equilibrium (m) |
| $s_E$ | elastic compliance (6 × 6 matrix; $m^2$ $N^{-1}$) in a constant electric field |
| $\mathbf{S}$ | strain vector (6 × 1 matrix; m $m^{-1}$) |
| $\mathbf{T}$ | stress vector (6 × 1 matrix; Pa) |
| t | time (s) |
| $\mathbf{u}$ | particle displacement (m) |
| x | defined power series |

Greek letters

| | |
|---|---|
| $\alpha$ | characteristic exponent |
| $\beta$ | ratio of driving frequency to bubble oscillation frequency |
| $\gamma$ | ratio of specific heats |
| $\varepsilon_S$ | dielectric permittivity matrix (3 × 3; F $m^{-1}$) at constant mechanical strain |
| $\varepsilon_T$ | dielectric permittivity matrix (3 × 3; F $m^{-1}$) at constant mechanical stress |
| $\mu$ | fluid viscosity (Pa s) |
| $\rho$ | water density (kg $m^{-3}$) |
| $\rho_m$ | material density (kg $m^{-3}$) |
| $\rho_s$ | density of horn rod (kg $m^{-3}$) |
| $\sigma$ | surface tension (N $m^{-1}$) |
| $\varphi$ | phase difference (rad) |

$\varphi_i$ phase difference for $i^{th}$ harmonic (rad)

$\omega$ angular frequency (rad $s^{-1}$)

## 1. Introduction

Many laboratory studies have reported the chemical processing of materials, water contaminants, and waste streams using ultrasound [1-3]. However, few studies report methods to scale up these bench-scale studies to larger systems. The most commonly used bench-scale device (e.g., horn type probe) for sonication has low energy efficiency, localized cavitation, and a non-uniform acoustic field in the reactor [4-6]. In our previous work, a scaled-up multi-stepped horn was designed and characterized showing higher energy efficiency, multiple cavitational zones, and more widely distributed acoustic pressure as compared to typical horns [7]. To date, there are still limited strategies that have been investigated to design new ultrasonic devices [7, 8], improve reactor performance [9-12], and scale up sonolytic processes [13, 14].

In the design process, computational simulations are used to investigate how different reactor geometries, horn configurations, and operational parameters (e.g., frequency) impact optimizing performance of ultrasonic systems [15-20]. Of the available computational tools, COMSOL Multiphysics applies a finite element method to solve different physics and engineering problems (e.g., acoustic propagation and heat transfer) governed by partial differential equations (PDEs). The numerous modules and corresponding analytical solutions in the software allow it to combine different phenomena into one model, which is required to simulate ultrasonic systems that feature electromechanical and elastic mechanical effects [21, 22]. Therefore, COMSOL Multiphysics has been applied to simulate acoustic fields and sonochemistry in reactors and has provided results consistent with laboratory measurements [15, 16, 18].

A hydrophone is a piezoelectric device that detects sound pressure underwater and converts the pressure signals to electrical signals. Hydrophone measurements are used to determine an acoustic pressure distribution in solution and through frequency spectral analysis, locate cavitation regions [23-25]. Bubble oscillations in an acoustic field, together with shock waves/micro-jets that follow bubble collapse, introduce many subharmonic/harmonic frequencies and a broad range of frequencies (i.e., background noise) [26-29]. This emitted broadband signal is indicative of transient cavitation [30]. Hydrophone measurements of acoustic emissions have been used to characterize acoustic fields and sonochemical reactivity in many ultrasonic systems [23, 30, 31].

The coupling of computational simulation with mapping the acoustic field using hydrophone measurements provides a method for designing ultrasonic reactors. This work presents a protocol for a sono-reactor design using this coupled method. First, acoustic field surrounding the newly designed multi-stepped horn was simulated in COMSOL Multiphysics to evaluate ultrasound propagation and the resulting cavitation zone in water. The simulation results were then verified using acoustic pressure maps from hydrophone measurements in a plexiglass box, followed by spectral analysis of ultrasound signals to determine the cavitation region and scope. Finally, the configuration of an approximately sized sono-reactor was proposed and modeled. We propose this method for reactor design as a rational way to design and characterize sono-reactors.

## 2. Methodology

### *2.1 COMSOL Simulation*

An ultrasonic system, composed of a transducer and a horn, involves different physical phenomena [6, 21, 22]. The piezoelectric material in the transducer converts electricity into mechanical vibrations which pass through the ultrasonic horn rod and are amplified at the end of the horn [22]. These amplified mechanical waves (i.e., ultrasonic waves) are emitted and propagate through a medium, such as water. Thus, three different modules were selected to simulate these physical effects in the COMSOL Multiphysics software (version 4.2): 1) a piezoelectric material module for the transducer; 2) a linear elastic material module for the horn rod; and 3) a pressure acoustics module for water [32, 33]. Each module is governed by its own equations that describe the specific physics as discussed in the following section.

#### 2.1.1 Applied physical modules

A piezoelectric effect is a phenomenon in which an applied stress on a piezoelectric material induces electric polarization or an applied electric field induces a dimensional change in the piezoelectric material [34]. In an ultrasonic transducer, the piezoelectric material, often a lead zirconate titanate (PZT) ceramic, generates a mechanical strain under an applied electrical field (i.e., alternating current or AC). Thus, these electromechanical behaviors of the isotropic PZT are expressed by linearized constitutive equations as follows [34, 35]:

$$\begin{cases} \mathbf{T} = c_E\mathbf{S} - e^t\mathbf{E} \\ \mathbf{D} = e\mathbf{S} + \varepsilon_S\mathbf{E} \end{cases} \tag{1a}$$

$$\begin{cases} \mathbf{S} = s_E\mathbf{T} + d^t\mathbf{E} \\ \mathbf{D} = d\mathbf{T} + \varepsilon_T\mathbf{E} \end{cases} \tag{1b}$$

where $\mathbf{T}$ is the stress vector (6 × 1 matrix; Pa), $\mathbf{S}$ is the strain vector (6 × 1 matrix; m $m^{-1}$), $\mathbf{E}$ is the electric field intensity vector (3 × 1 matrix; V $m^{-1}$), $\mathbf{D}$ is the electric flux density vector (3 × 1 matrix; C $m^{-2}$), $c_E$ is the elastic coefficient (6 × 6 matrix; Pa) at constant electric field strength, $e^t$ is the transposed dielectric permittivity matrix (6 × 3; C $m^{-2}$), e is the dielectric permittivity (3 × 6 matrix; C $m^{-2}$), $\varepsilon_S$ is the dielectric permittivity matrix (3 × 3; F $m^{-1}$) at constant mechanical strain, $s_E$ is the elastic compliance (6 × 6 matrix; $m^2$ $N^{-1}$) in a constant electric field, $d^t$ is the transposed piezoelectric strain constant matrix (6 × 3; m $V^{-1}$), d is the piezoelectric strain constant (3 × 6 matrix; m $V^{-1}$), and $\varepsilon_T$ is the dielectric permittivity matrix (3 × 3; F $m^{-1}$) at constant mechanical stress.

The vibration generated in the piezoelectric transducer is then transmitted to the horn rod. Assuming both the stainless steel structure of the horn rod and PZT are isotropic and elastic, their linear elastic behavior is governed by Newton's Second Law [32, 33]:

$$-\rho_m \omega^2 \mathbf{u} - \nabla \cdot \mathbf{T} = \mathbf{F}_V e^{i\phi} \quad (2)$$

where $\rho_m$ is the material density (kg m$^{-3}$), $\omega$ is the angular frequency (rad s$^{-1}$), $\mathbf{u}$ is the particle displacement (m), $\mathbf{F}_V$ is the force per volume (N m$^{-3}$), and $e^{i\phi}$ indicates the AC.

The pressure acoustics module has been used to simulate ultrasound propagation in water. The acoustic wave equation is given as follows [33, 35, 36]:

$$\nabla \cdot \left( -\frac{1}{\rho} \nabla P + \mathbf{q} \right) + \frac{\omega^2 P}{\rho c^2} = 0 \quad (3)$$

where $\rho$ is the density of water (kg m$^{-3}$), $c$ is the speed of ultrasound propagation in water (m s$^{-1}$), $P = P_A \cos(\omega t)$ is the acoustic pressure (Pa; $P_A$ is the maximum acoustic pressure and $t$ is time, s), and the dipole source $\mathbf{q}$ (m s$^{-2}$) is optional. For our setup, there is no polarization ($\mathbf{q}$ = 0) for the longitudinal ultrasonic waves [36].

2.1.2 Assigned boundary conditions and initial inputs

The boundary conditions set to couple the three modules are based on COMSOL Modeling Guides [32, 33] and previous simulation studies [16, 18]. A structure-acoustic boundary was set to the interface between the ultrasonic horn and water [33, 37].

Specifically, the movement of the horn and surrounding solution was coupled at the interface:

$$\mathbf{n} \cdot \left( -\frac{1}{\rho_s} \nabla P + \mathbf{q} \right) = a_n \quad (4)$$

where $\mathbf{n}$ is the normal unit vector, $\rho_s$ is the density of horn (kg $m^{-3}$), and $a_n$ is the normal acceleration of the solution (m $s^{-2}$). Likewise, the stress exerted from the surrounding solution on the horn is subjected to the acoustic pressure changes in the solution as follows:

$$T \cdot \mathbf{n} = P \cdot \mathbf{n} \quad (5)$$

Displacements at the interface between the water and the wall of the tank were set to zero ($\mathbf{u} = 0$ or $P = 0$), assuming the tank material with a large acoustic impedance sufficiently absorbed incident ultrasonic waves. Boundary conditions for surfaces contacting air were also set to $P = 0$ [33]. The displacement at the joint between the piezoelectric material and the stainless steel horn was set to the same value [8, 38, 39]. The default temperature was 293.15 K. The liquid, horn, and transducer domains were assigned to linear water media, piezoelectric material (PZT-5H), and stainless steel material (AISI 4340), respectively. The input information of these materials is summarized in Table S1 of supporting information (SI).

### *2.2 Experimental Verification*

#### 2.2.1 Ultrasonic system

As shown in Fig. S1, a Branson BCA 900 series power supplier (1000 W at maximum) was used to transmit electrical power to a Branson 902R Model ultrasonic transducer (20 kHz) which was connected to a multi-stepped horn. The ultrasonic horn was placed at the center of a water tank (61 cm × 61 cm × 45 cm, 167.5 L) made of plexiglass. A Reson TC4013 type hydrophone (Reson A/S, Denmark) was used to measure acoustic pressure in the water tank. The hydrophone was connected to a TDS 5000 Tektronix oscilloscope (Tektronix Inc., USA) which recorded and displayed the sound signals at a sampling frequency of 125 kHz. Another typical horn-type ultrasonic system (Sonic Dismembrator 550, Fisher Scientific) was used to determine the cavitation threshold following the method of Ashokkumar et al. [30].

#### 2.2.2 Experimental procedure

Approximately 150 L of water was filled to a depth of 40 cm in the plexiglass tank and was left overnight allowing for air saturation. The multi-stepped horn was submerged to the depth of 16 cm (from horn tip to water surface). The depth right below the horn tip was defined to be Z = 0 and horizontal planes were defined as X-Y planes. A manual positioning system with a resolution of 2 cm was used to position the hydrophone accurately during acoustic field mapping. The origin of the hydrophone was just below the horn tip (X, Y, Z = 0, 0, 0). With the manual positioning system, the hydrophone was then moved in the X-Y plane at 2 cm intervals, followed by movements in the Z-direction (vertical) to map another X-Y plane. A full-scan of an X-Y plane was accomplished through line scans in the x- or y-axis. X-Y planes below the horn tip (Z = –4 cm), at the horn tip (Z = 0 cm), and above the horn tip (Z = +4 cm) were scanned to generate acoustic field maps for the multi-stepped horn in the water tank. Hydrophone readings in these scans were acquired as root mean square values by the oscilloscope. Operational conditions such as power input and water volume were constant for all measurements. The temperature of water in the tank varied from 18 ºC to 22 ºC depending on the length of sonication. Such temperature change was not found to alter hydrophone readings.

### *2.3 Acoustic Emission*

The acoustic emission method was used to determine the cavitation region in the hydrophone-mapped acoustic field. Frequency is a critical factor to determine the shape of a sound signal. At low power intensity, a sinusoidal shape for a sound signal converted from AC indicates one dominant frequency (i.e., 20 kHz in our system) and a linear vibration for bubbles. When a high intensity distorts the linear system, multiples of the driving frequency (i.e., ultraharmonics) are generated [40]. Beyond a threshold value, subharmonics appear [40]. The numerical analysis of bubble oscillation at subharmonic and ultraharmonic frequencies is explained in the SI. Collapse of cavitation bubbles induces shock waves and micro-jets forming a noisy background. These bubble oscillations and collapses generate a broadband signal (i.e., an elevated baseline), which is indicative of transient cavitation [41]. Both the elevated baseline and sharp peaks at the driving, subharmonic, and ultraharmonic frequencies are characteristics of an observed hydrophone spectrum from high power ultrasound. The frequency spectral analysis was carried out with PeakFit software (version 4.12) which uses a Fast Fourier Transform (FFT) algorithm. We assume that all sound signals and bubble dynamics are harmonic by using FFT. A wavelet transform algorithm, which analyzes sound signals in both time and frequency domains, needs to be used when bubble motions are not in steady state [42, 43].

## 3. Results and Discussion

### *3.1 Acoustic Field Modeling*

COMSOL simulations were first conducted to estimate ultrasound penetration distance and cavitation locations for the multi-stepped horn. The modeling result is a valuable reference for the subsequent experimental design. In the simulation, several assumptions were made: 1) there is no energy loss due to piezoelectric effects or transmission of mechanical energy from the transducer to the horn rod; thus, simulation results may overestimate particle displacements for both the piezoelectric material and stainless steel horn rod; 2) the acoustic pressure distribution in the tank is symmetric and damping of the ultrasonic waves is neglected; 3) there are no cavitation bubbles generated in the tank; and 4) water movement in the tank is negligible.

In the construction of 2D half geometry model (Fig. S2), the ultrasonic horn irradiates water in a cylindrical volume with a diameter of 31 cm and a height of 36 cm. Fig. 1 shows the simulated acoustic pressure distribution in an X-Z plane (vertical) where red or blue indicates a high absolute acoustic pressure. Due to the propagation of ultrasonic waves, the red and blue colors oscillate temporally in those regions. Therefore, the term “high acoustic pressure region” indicates both red and blue areas unless noted otherwise. As shown in Fig. 1, high acoustic pressure regions surrounding the horn neck and below its tip were observed. At regions further from the probe, ultrasonic waves propagate in the water forming ripples. The acoustic pressure decreases from the center to the edges due to the wave interactions at the boundaries where displacement of tank material was set to zero. Thus, color changes from red to yellow and blue to cyan in the acoustic pressure modeling simulations reflect the effect of constructive/destructive interferences that are induced by the wave interaction between the multi stepped horn and the geometrical characteristics of the vessel. Fig. 2 compares acoustic fields in X-Y planes at different depths, where plane 3 is at $Z = 0$ cm. Ultrasonic waves emitting from the horn neck generate a large high acoustic pressure region in plane 2. In plane 2, the distance of the dark-colored region extends to approximately 10 cm as opposed to $\leq 5$ cm in other X-Y planes. The simulated acoustic pressure maps indicate that areas surrounding the ultrasonic horn neck ($Z > 0$ cm) are more likely to generate multiple cavitation zones and increase cavitation volumes.

*3.2 Acoustic Field Mapping*

The acoustic pressure distribution surrounding the multi-stepped horn was verified using hydrophone measurements in the plexiglass tank. Hydrophone readings were recorded as root mean square values. Thus, values are reported as positive values as opposed to alternating values shown in simulations. First, the acoustic pressure from Z = – 15 cm to Z = + 15 cm was measured at different distances to the horn neck (i.e., 2 cm, 5 cm, and 10 cm), as shown in Fig. 3. Apparently, the radial region of the horn neck ($0 \leq Z \leq + 15$cm) exhibited higher acoustic pressure compared to the regions below the horn tip. The fluctuating pressure magnitudes along the multi-stepped horn suggest that the constructive interference of ultrasonic waves resulted in a high acoustic pressure region while destructive interference resulted in a low pressure region [44-46]. In addition, the acoustic pressure decayed with distance (2 cm > 5 cm > 10 cm) consistent with the simulated ultrasound propagation in Fig. 2. However, the higher power input does not intensify the acoustic pressure. This unexpected observation probably reflects the scattering of sound by a large amount of cavitation bubbles thereby reducing sound propagation [23]. Such a nonlinear relationship between acoustic pressure and power input has also been observed in previous studies [23, 47]. They attributed the nonlinearity to the acoustic energy dissipated into frequencies beyond the hydrophone detection limit and the shielding effect of cavitation bubbles that limits the propagation of ultrasound in water-filled vessels.

In addition to vertical mapping, horizontal propagation of ultrasonic waves in water is also depicted in 3D and contour plotting (Fig. 4). As shown in Fig. 4, a decreasing intensity from the tank center to its edges was observed. Particularly at Z = 0 cm, it was obvious that the center area below the horn tip exhibited the highest acoustic pressure levels; at Z = +4 cm, the horn neck emitted ultrasonic waves and created a large high acoustic pressure region; at Z = –4 cm, the acoustic pressure distribution was more dispersed without obvious spots of higher intensity. The observation of a larger scale of high pressure region at $Z > 0$ cm and a more discrete distribution of acoustic pressures at $Z \leq 0$ cm were consistent with the simulation results in Fig. 2. However, a standing wave pattern of propagation was not observed due to the following acoustic effects [23, 48]: 1) cavitation shielding due to the presence of cavitation bubbles interferes with ultrasound propagation (e.g., sound intensity attenuation and sound velocity reduction resulting from scattering at the bubble-water interface); 2) collisions between emitted ultrasonic waves from the horn neck and reflected waves from the tank wall disrupt the applied acoustic pressure; and 3) agitation of water by acoustic streaming drifts vibrating molecules off their original positions resulting in the discrete and asymmetric distribution of acoustic pressure. Hodnett et al. [23] also show an asymmetric but reproducible distribution of the acoustic field in the characterization of a reference ultrasonic cavitation vessel. Mhetre and Gogate [49] in recent work present a non-uniform cavitation activity distribution in traditional dosimetry tests using potassium iodide (KI) in a large-scale sonochemical reactor (72 L in volume). It seems hydrophone measurements are capable of generating acoustic field maps consistent with traditional chemical methods.

*3.3 Cavitation Threshold and Reactive Region*

After mapping the acoustic field in the large water tank, the next step was to evaluate the effective range of the cavitation zones based on the threshold value of cavitation which was determined using acoustic emissions. Fig. 5 shows acoustic waveforms acquired on the oscilloscope and the corresponding spectra. The waveforms are sinusoidal to irregular in shape and become more irregular with increasing acoustic intensity (< 0.04 – 1.16 W $cm^{-2}$). In an ideal system, the sinusoidal AC input is converted via a transducer into a sinusoidal vibration that is propagated through the ultrasonic horn to aqueous solution. Without dissipation, water movement and cavitation bubbles, the hydrophone captures a sinusoidal sound signal that is displayed on the oscilloscope. With increasing power input, bubble oscillations depart from this linear nature producing convex waveforms (Fig. 5). The addition of shock waves, micro-jets, and micro-streaming after collapse of cavitation bubbles further increases the degree of irregularity of acoustic waveforms.

Frequency spectra in Fig. 5 are consistent with the waveforms. At low power intensities, the driving frequency (f) and ultraharmonic frequency (2f) were observed. As power intensity was increased (≥ 0.04 W $cm^{-2}$), subharmonic frequencies were also present. The number of subharmonic and ultraharmonic frequencies increased significantly at a power intensity of 0.31 W $cm^{-2}$. At 0.74 W $cm^{-2}$, the baseline was elevated to a magnitude of approximately 10, showing the feature of a broadband signal that is an indicator of transient cavitation [30]. Therefore, transient cavitation is present at power intensities of 0.74 W $cm^{-2}$ and higher, which is similar to 0.70 W $cm^{-2}$ observed by Ashokkumar et al. [30]. While the threshold is somewhere between 0.31 W $cm^{-2}$ and 0.74 W $cm^{-2}$, we defined the acoustic intensity of 0.74 W $cm^{-2}$ as the "threshold" for transient cavitation, which corresponds to a hydrophone reading of 0.63 Volt. Even though this defined threshold may underestimate the power intensity of transient cavitation, setting a threshold slightly high ensures necessary properties for a sufficient design.

Using the cavitation threshold defined, a cavitation zone was identified. As shown in Fig. 3, the threshold for transient cavitation was plotted as a red dotted line. The measurements higher than the cavitation threshold were generally located between Z = 0 cm and Z = +15 cm which is along the neck of the horn. The cavitation region along the neck (Z > 0 cm) extended up to 10 cm from the horn axis while the cavitation zone below the horn tip ($Z \leq 0$ cm) extended up to 5 cm laterally from the axis (75% and 100% power inputs). At 50% power input, up to 10 cm of cavitation region was also observed right below the horn tip ($-5$ cm $< Z \leq 0$ cm) reconfirming the shielding effect of cavitation bubbles. In Fig. 4, regions higher than the cavitation threshold are cyan and warmer colors. At Z = +4 cm, there was a large area with cyan to red colors surrounding the horn neck. In contrast, the cavitation zones were much smaller at Z = 0 cm and Z = –4 cm. In order to quantitatively describe the cavitation regions in an X-Y plane, the ratio of collected data points higher than the threshold value to the total number of scanned points was calculated (Fig. 6). At Z = +4 cm, the cavitation zone covered > 85.0% of a 10 cm × 10 cm area. The percentage of the zone above the transient cavitation threshold dropped to 73.2% and 49.5% when distances were extended to 12 cm and 20 cm from the horn axis, respectively. If > 85% is selected as a reasonable percentage of a zone undergoing transient cavitation in the reactor, a cylindrically-shaped reactor with a 10 cm radius would be designed to fit the multi-stepped horn. In the X-Y planes that did not cross the horn neck, the percentage of cavitation zones dropped dramatically. For example, at 10 cm from the horn axis, the percentage of cavitation zones was 47.9% and 26.4% for $Z = 0$ cm and $Z = -4$ cm, respectively. Even though a relatively low percentage was observed at $Z \leq 0$ cm, both X-Y planes featured a high acoustic pressure center below the horn tip. Thus, a shrinking shaped bottom, such as a conical shape, could be introduced to the reactor design to increase the percentage of total cavitation volume. In addition, a cone-shaped bottom is beneficial for solution circulation and mass transfer inside the reactor, as verified in our previous studies [50, 51].

With those conditions considered, we propose a cylindrically-shaped reactor with a 10 cm diameter and a conical bottom with 5 cm in depth (21 cm in total depth). As shown in frame 8 of Fig. 7, the treatment volume for this design was approximately 5.0 L, which is nearly 100-fold greater than the reactor volume for a typical ultrasonic horn [50, 51]. We further verified the design using COMSOL software. Using COMSOL we simulated the acoustic pressure distribution and ultrasound propagation (frame 1-7 in Fig. 7) in the reactor. As shown in Fig. 7, the majority of the reactor was covered by high acoustic pressure regions in red (up to $+1.59 \times 10^5$ Pa) and blue (down to $-1.59 \times 10^5$ Pa) colors suggesting that multiple reactive zones exist and a large cavitation volume can be generated in the reactor if applying high intensity ultrasound. The animation of pressure propagation starts in frame 1 and ends at frame 7. Frames 1 and 7 are identical indicating a complete cycle of propagation. The cyclic propagation of ultrasound suggests a reproducible acoustic pressure distribution which is a key design factor for sono-reactors.

## 4. Applications and Limitations

This study describes a method of using COMSOL simulations and acoustic pressure mapping from hydrophone measurements for sono-reactor design. The COMSOL simulations showed regions of high acoustic pressure similar to the acoustic pressure maps created in the plexiglass tank, suggesting this coupling method may be used as a tool in the design and characterization of an ultrasonic system. In addition, the multi-stepped horn with a 10 cm radiation radius and 5.0 L treatment capacity with a high expected amount of cavitation in the reactor shows great potential for large-scale applications through an array of these horns. The next step is to build the sono-reactor with this proposed configuration and quantitatively evaluate its performance through traditional calorimetry, dosimetry, and sonochemical processing of a model compound.

Although the overall trends of simulated acoustic pressure maps are consistent with experimental measurements, accurate modeling of these systems needs further development. First of all, an immediate challenge for future COMSOL simulations is to couple bubble dynamics with the acoustic wave equation. Kumar et al. utilized a continuum mixture model and a diffusion limited model to explore the behavior of cavitation bubbles in a flow, suggesting a possible methodology to couple bubble dynamics with the acoustic wave equation in a sono-reactor [52, 53]. Second, a simplified transducer was created in current simulations (Fig. S2). Modeling of the transducer to reflect its inside structure is beyond the scope of this paper, but is an aspect to be developed in future studies. In addition, ideal conditions were applied for all physical modules used and reactor material was not considered in the simulations. The material and shape used may have a significant impact in the reactor design because absorption and reflection of incident waves on the reactor wall will change the acoustic pressure distribution in the reactor. Therefore, incorporating necessary properties such as water viscosity, heat production, cavitation bubbles, cavitation shielding, and reactor materials into simulations is necessary to improve simulation results.

**Acknowledgments**

This work was supported by the Office of Naval Research (ONR Contract No. N00014-04-C-0430) and Ohio Sea Grant College Program.

## References

[1] T.J. Mason, J.P. Lorimer, Applied Sonochemistry: The Use of Power Ultrasound in Chemistry and Processing, Wiley-VCH, Verlag GmbH, Weinheim, 2002.

[2] K.S. Suslick, Ultrasound: Its Chemical, Physical, and Biological Effects. VCH Publishers, New York, 1988.

[3] R.Y. Xiao, Z.S. Wei, D. Chen, L.K. Weavers, Kinetics and mechanism of sonochemical degradation of pharmaceuticals in municipal wastewater, Environ. Sci. Technol. 48 (2014) 9675-9683.

[4] D. Chen, L.K. Weavers, H.W. Walker, Ultrasonic control of ceramic membrane fouling by particles: Effect of ultrasonic factors, Ultrason. Sonochem. 13 (2006) 379-387.

[5] H.N. McMurray, B.P. Wilson, Mechanistic and spatial study of ultrasonically induced luminol chemiluminescence, J. Phys. Chem. A. 103 (1999) 3955-3962.

[6] J.M. Mason, A. Tiehm, Advances in Sonochemistry, Jai Press, Connecticut, 2001.

[7] Z. Wei, J.A. Kosterman, R. Xiao, G.Y. Pee, M. Cai, L.K. Weavers, Designing and characterizing a multi-stepped ultrasonic horn for enhanced sonochemical performance, Ultrason. Sonochem. 27 (2015) 325–333.

[8] S.L. Peshkovsky, A.S. Peshkovsky, Matching a transducer to water at cavitation: Acoustic horn design principles, Ultrason. Sonochem. 14 (2007) 313-322.

[9] S.I. Nikitenko, C. Le Naour, P. Moisy, Comparative study of sonochemical reactors with different geometry using thermal and chemical probes, Ultrason. Sonochem. 14 (2007) 330-336.

[10] J. Rooze, E.V. Rebrov, J.C. Schouten, J.T.F. Keurentjes, Effect of resonance frequency, power input, and saturation gas type on the oxidation efficiency of an ultrasound horn, Ultrason. Sonochem. 18 (2011) 209-215.

[11] V.S. Sutkar, P.R. Gogate, Design aspects of sonochemical reactors: Techniques for understanding cavitational activity distribution and effect of operating parameters, Chem. Eng. J. 155 (2009) 26-36.

[12] R. Xiao, D. Diaz-Rivera, L.K. Weavers, Factors influencing pharmaceutical and personal care product degradation in aqueous solution using pulsed wave ultrasound, Ind. Eng. Chem. Res. 52 (2013) 2824-2831.

[13] P.R. Gogate, V.S. Sutkar, A.B. Pandit, Sonochemical reactors: important design and scale up considerations with a special emphasis on heterogeneous systems, Chem. Eng. J. 166 (2011) 1066-1082.

[14] T.J. Mason, A. Collings, A. Sumel, Sonic and ultrasonic removal of chemical contaminants from soil in the laboratory and on a large scale, Ultrason. Sonochem. 11 (2004) 205-210.

[15] L. Csoka, S.N. Katekhaye, P.R. Gogate, Comparison of cavitational activity in different configurations of sonochemical reactors using model reaction supported with theoretical simulations, Chem. Eng. J. 178 (2011) 384-390.

[16] J. Klima, A. Frias-Ferrer, J. Gonzalez-Garcia, J. Ludvik, V. Saez, J. Iniesta, Optimisation of 20 kHz sonoreactor geometry on the basis of numerical simulation of

local ultrasonic intensity and qualitative comparison with experimental results, Ultrason. Sonochem. 14 (2007) 19-28.

[17] F.J. Trujillo, K. Knoerzer, A computational modeling approach of the jet-like acoustic streaming and heat generation induced by low frequency high power ultrasonic horn reactors, Ultrason. Sonochem. 18 (2011) 1263-1273.

[18] Y.C. Wang, M.C. Yao, Realization of cavitation fields based on the acoustic resonance modes in an immersion-type sonochemical reactor, Ultrason. Sonochem. 20 (2013) 565–570.

[19] R. Jamshidi, B. Pohl, U. Peuker, G. Brenner, Numerical investigation of sonochemical reactors considering the effect of inhomogeneous bubble clouds on ultrasonic wave propagation, Chem. Eng. J. 189-190 (2012) 364– 375.

[20] R.Y. Xiao, M. Noerpel, H.L. Luk, Z.S. Wei, R. Spinney, Thermodynamic and kinetic study of ibuprofen with hydroxyl radical: A density functional theory approach, Int. J. Quantum. Chem. 114 (2014) 74-83.

[21] N. Feng, Ultrasonics Handbook, first ed., Nanjing University Press, Nanjing, 1999.

[22] K.F. Graff, Wave Motion in Elastic Solids, Dover Publications, Inc., New York, 1975.

[23] M. Hodnett, M.J. Choi, B. Zeqiri, Towards a reference ultrasonic cavitation vessel. Part 1: Preliminary investigation of the acoustic field distribution in a 25 kHz cylindrical cell, Ultrason. Sonochem. 14 (2007) 29-40.

[24] M. Hodnett, B. Zeqiri, A strategy for the development and standardisation of measurement methods for high power cavitating ultrasonic fields: review of high power field measurement techniques, Ultrason. Sonochem. 4 (1997) 273-288.

[25] M. Juschke, C. Koch, Model processes and cavitation indicators for a quantitative description of an ultrasonic cleaning vessel: Part I: Experimental results, Ultrason. Sonochem. 19 (2012) 787-795.

[26] J. Frohly, S. Labouret, C. Bruneel, I. Looten-Baquet, R. Torguet, Ultrasonic cavitation monitoring by acoustic noise power measurement, J. Acoust. Soc. Am. 108 (2000) 2012-2020.

[27] D.L. Miller, Ultrasonic detection of resonant cavitation bubbles in a flow tube by their 2nd-harmonic emissions, Ultrasonics. 19 (1981) 217-224.

[28] Y. Son, M. Lim, J. Khim, M. Ashokkumar, Acoustic emission spectra and sonochemical activity in a 36 kHz sonoreactor, Ultrason. Sonochem. 19 (2012) 16-21.

[29] E. Cramer, W. Lauterborn, Acoustic cavitation noise spectra, Appl. Sci. Res. 38 (1982) 209-214

[30] M. Ashokkumar, M. Hodnett, B. Zeqiri, F. Grieser, G.J. Price, Acoustic emission spectra from 515 kHz cavitation in aqueous solutions containing surface-active solutes, J. Am. Chem. Soc. 129 (2007) 2250-2258.

[31] G.J. Price, M. Ashokkumar, M. Hodnett, B. Zequiri, F. Grieser, Acoustic emission from cavitating solutions: Implications for the mechanisms of sonochemical reactions, J. Phys. Chem. B. 109 (2005) 17799-17801.

[32] COMSOL, Acoustics Module User's Guide, version 4.2, 2012.

[33] COMSOL, COMSOL Multiphysics modeling guide, version 4.2, 2012.

[34] S.O.R. Moheimani, A.J. Fleming, Piezoelectric Transducers for Vibration Control and Damping, Oxford University Press, Oxford, UK, 2006.

[35] M.W. Nygren, Finite element modeling of piezoelectric ultrasonic transducers, Master thesis, Norwegian University of Science and Technology, 2011.

[36] L.E. Kinsler, A.R. Frey, A.B. Coppens, J.V. Sanders, Fundamentals of Acoustics, fourth ed. , John Wiley & Sons, New York, NY, 2000.

[37] M. Yao, Analysis and experiment of resonant sonochemical cell, Master thesis, National Cheng Kung University, 2009.

[38] Z.Q. Fu, X.J. Xian, S.Y. Lin, C.H. Wang, W.X. Hu, G.Z. Li, Investigations of the barbell ultrasonic transducer operated in the full-wave vibrational mode, Ultrasonics. 52 (2012) 578-586.

[39] Z. Lin, Theory and Desing of Ultrasonic Horn, Science Press, Beijing, 1987.

[40] A. Eller, H.G. Flynn, Generation of subharmonics of order one-half by bubbles in a sound field, J. Acoust. Soc. Am. 46 (1969) 722-727.

[41] E.A. Neppiras, Subharmonic and other low-frequency emission from bubbles in sound-irradiated liquids, J. Acoust. Soc. Am. 46 (1969) 587- 601.

[42] V.S. Moholkar, M. Huitema, S. Rekveld, M.M.C.G. Warmoeskerken, Characterization of an ultrasonic system using wavelet transforms, Chem. Eng. Sci. 57 (2002) 617-629.

[43] V.S. Moholkar, S.P. Sable, A.B. Pandit, Mapping the cavitation intensity in an ultrasonic bath using the acoustic emission, AIChE J. 46 (2000) 684-694.

[44] S. Dahnke, F.J. Keil, Modeling of three-dimensional linear pressure fields in sonochemical reactors with homogeneous and inhomogeneous density distributions of cavitation bubbles, Ind. Eng. Chem. Res. 37 (1998) 848-864.

[45] S. Dahnke, K.M. Swamy, F.J. Keil, A comparative study on the modeling of sound pressure field distributions in a sonoreactor with experimental investigation, Ultrason. Sonochem. 6 (1999) 221-226.

[46] S.W. Dahnke, F.J. Keil, Modeling of linear pressure fields in sonochemical reactors considering an inhomogeneous density distribution of cavitation bubbles, Chem. Eng. Sci. 54 (1999) 2865-2872.

[47] M. Hodnett, R. Chow, B. Zeqiri, High-frequency acoustic emissions generated by a 20 kHz sonochemical horn processor detected using a novel broadband acoustic sensor: a preliminary study, Ultrason. Sonochem. 11 (2004) 441-454.

[48] K.W. Commander, A. Prosperetti, Linear pressure waves in bubbly liquids - Comparison between theory and experiments, J. Acoust. Soc. Am. 85 (1989) 732-746.

[49] A.S. Mhetre, P.R. Gogate, New design and mapping of sonochemical reactor operating at capacity of 72 L, Chem. Eng. J. 258 (2014) 69-76.

[50] Z.Q. He, S.J. Traina, J.M. Bigham, L.K. Weavers, Sonolytic desorption of mercury from aluminum oxide, Environ. Sci. Technol. 39 (2005) 1037-1044.

[51] G.Y. Pee, S. Na, Z. Wei, L.K. Weavers, Increasing the bioaccessibility of polycyclic aromatic hydrocarbons in sediment using ultrasound, Chemosphere. 122 (2015) 265–272.

[52] P. Kumar, S. Khanna, V.S. Moholkar, Flow regime maps and optimization thereby of hydrodynamic cavitation reactors, AIChE J. 58 (2012) 3858-3866.

[53] V.S. Moholkar, A.B. Pandit, Modeling of hydrodynamic cavitation reactors: a unified approach, Chem. Eng. Sci. 56 (2001) 6295-6302.

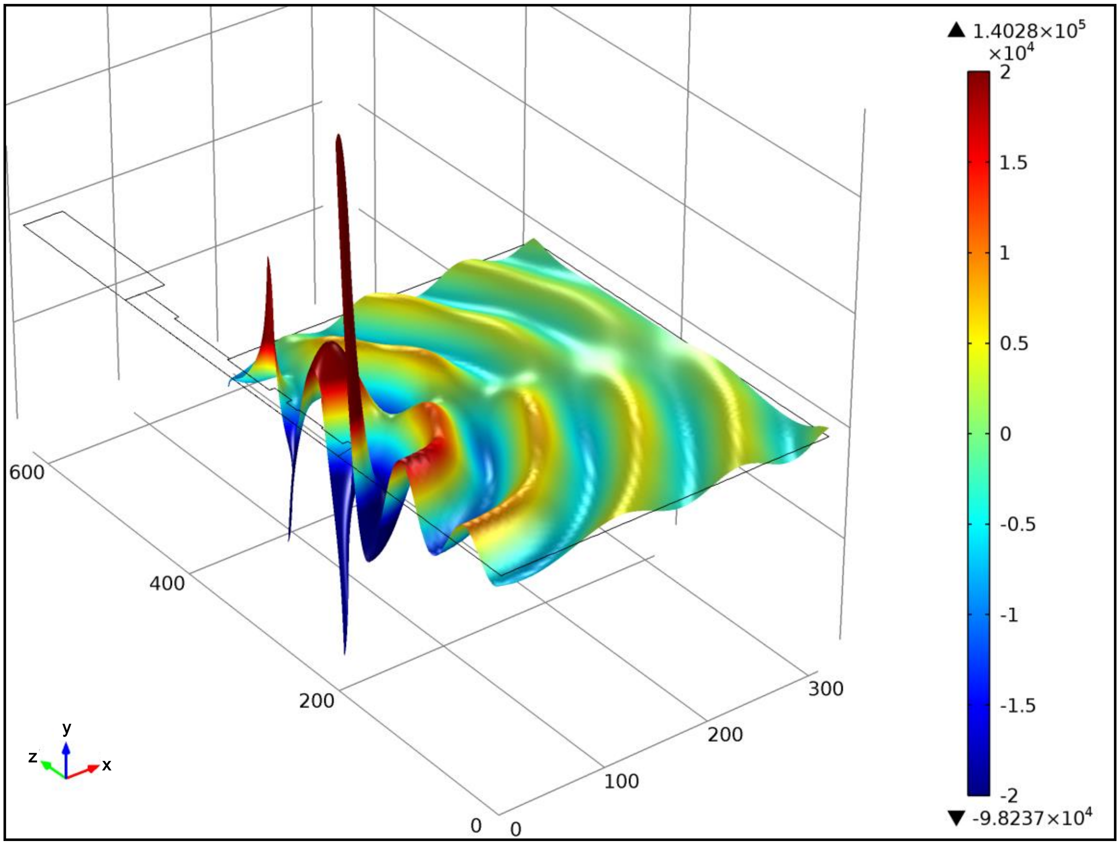


**Fig. 1.** Simulation of acoustic pressure distribution in X-Z plane (Units for color labels and axes are Pa and mm, respectively)

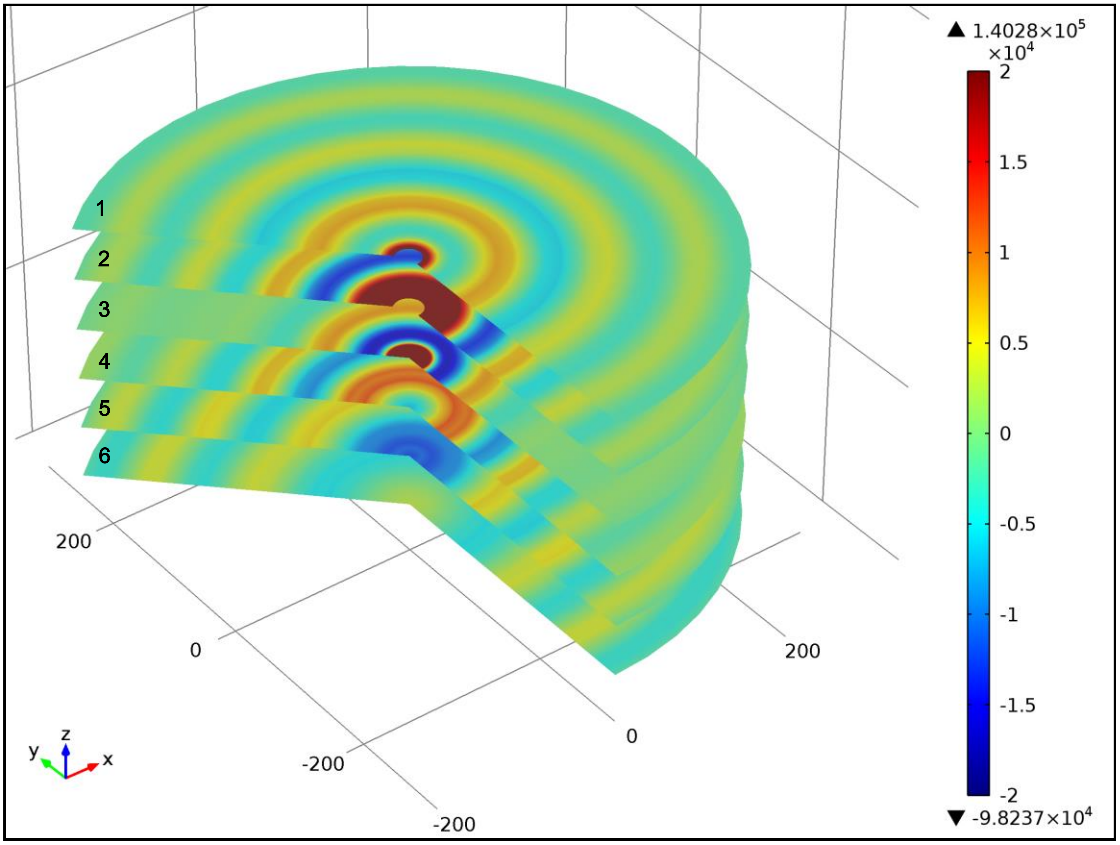


**Fig. 2**.Simulation of acoustic pressure distribution in X-Y planes at different depths (1 — X-Y plane near water surface; 2 — X-Y plane in the middle of horn neck; 3 — X-Y plane at Z = 0 cm; 4-6 — X-Y planes at Z < 0 cm; units for color labels and axes are Pa and mm, respectively)

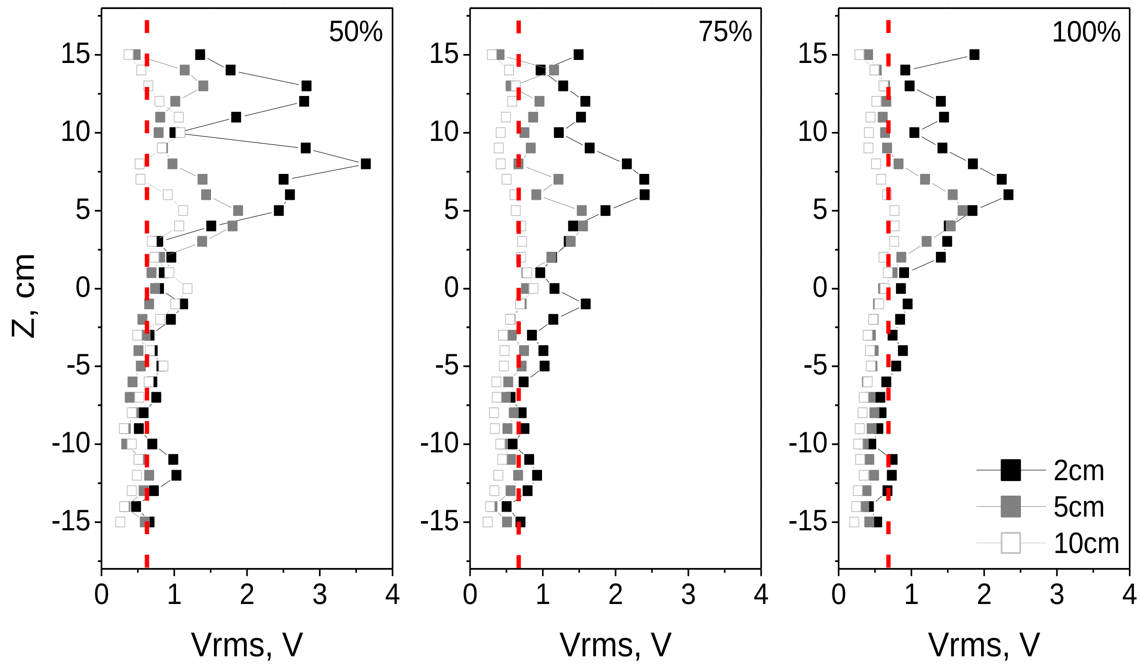


**Fig.3.** Acoustic pressure distribution in Z-direction at different distances (2 cm, 5 cm and 10 cm) and power levels (50%, 75% and 100%; red dotted line is the cavitation threshold value of 0.63 V)

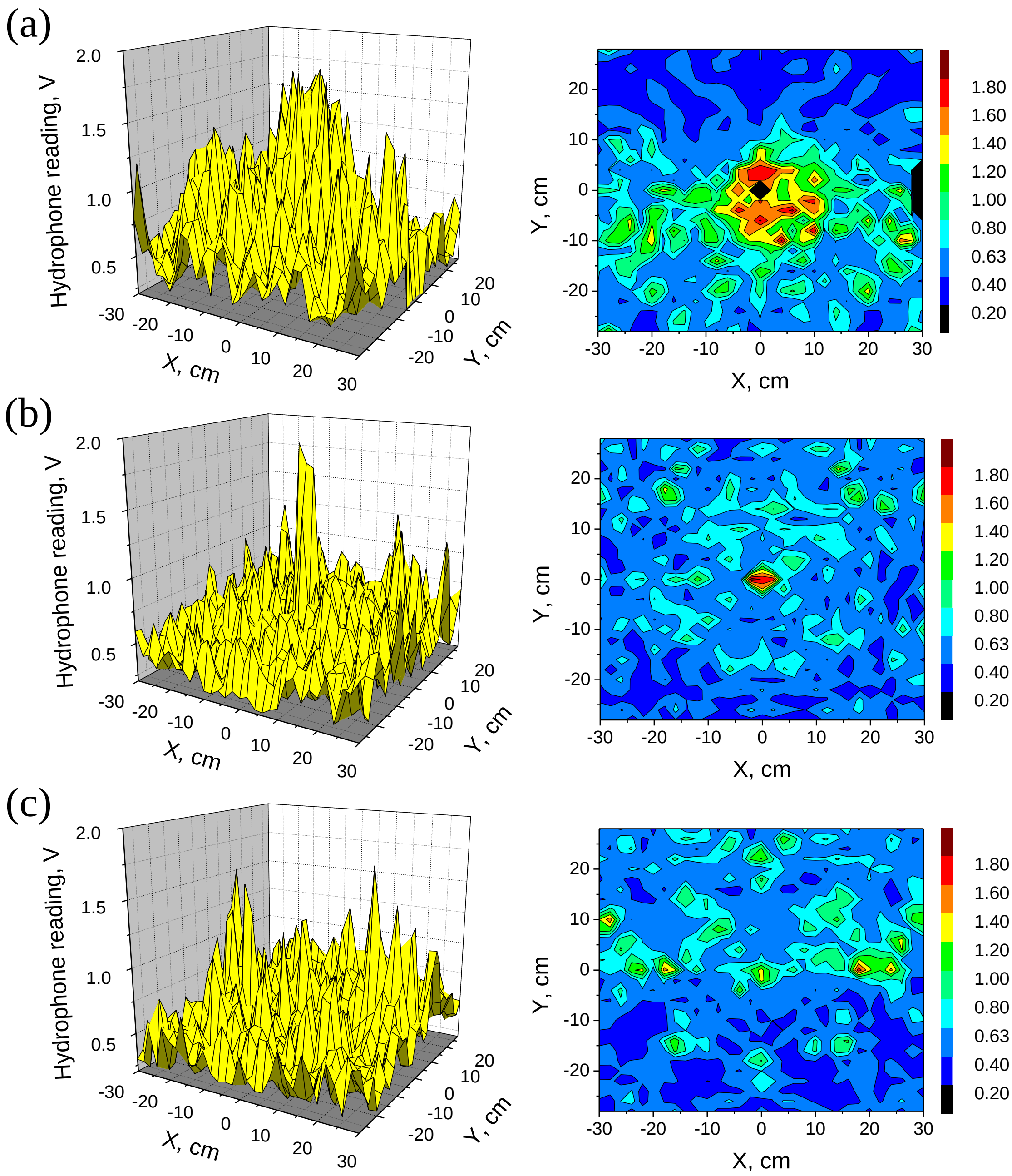


**Fig. 4.** 3D (left) and contour (right) mapping of hydrophone measurements in plexiglass tank (This scan was carried out at room temperature with 50% power input from power supply to transducer; a — X-Y plane at Z = +4 cm; b — X-Y plane at Z = 0 cm; c — X-Y plane at Z = –4 cm)

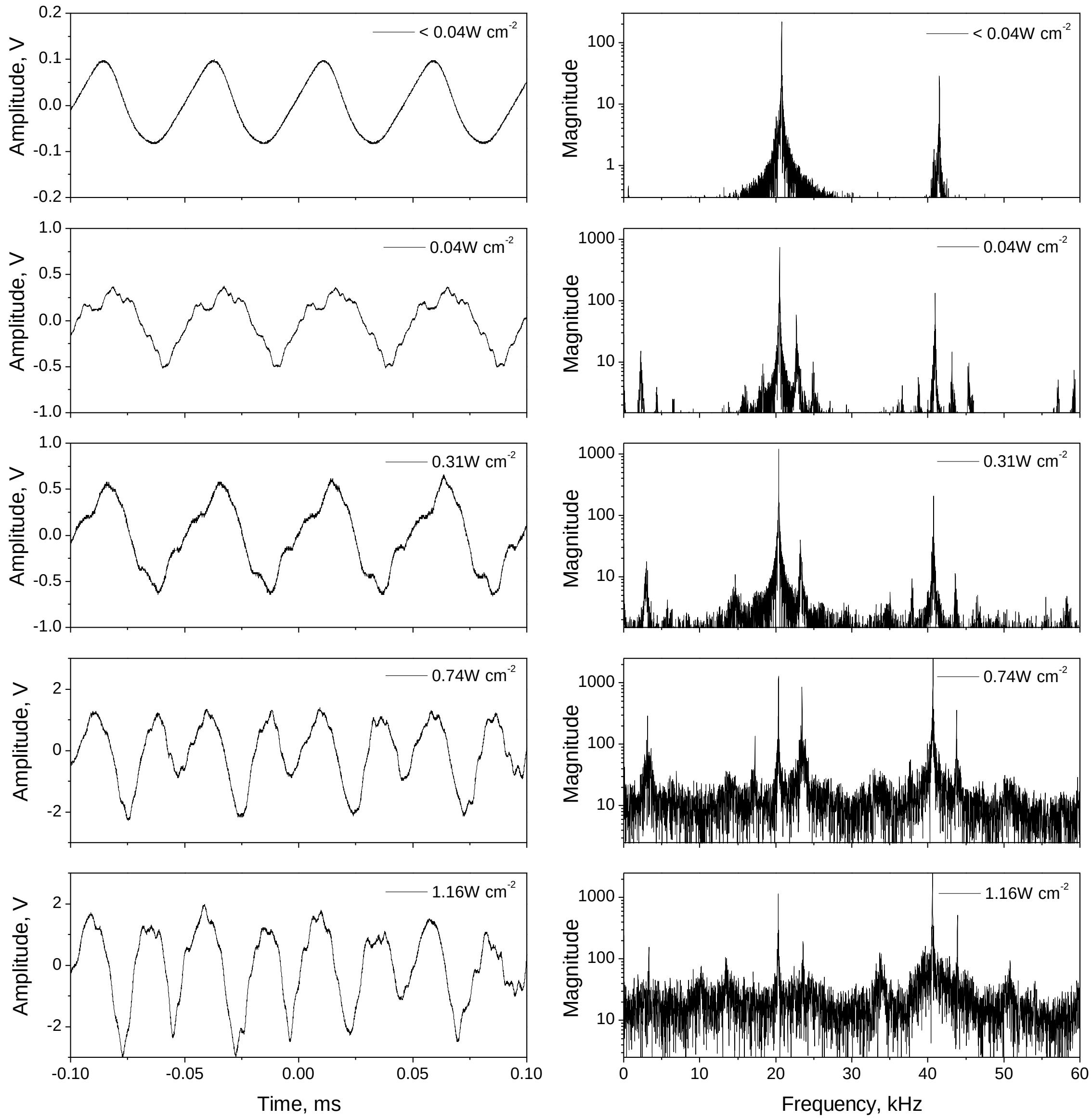


**Fig. 5.** Ultrasonic waveforms (left) and frequency spectra (right) observed in water at different power intensities (Convex feature in the waveform results from the sum of waveforms in different frequencies to the original waveform; units for magnitude of frequency spectra are arbitrary)

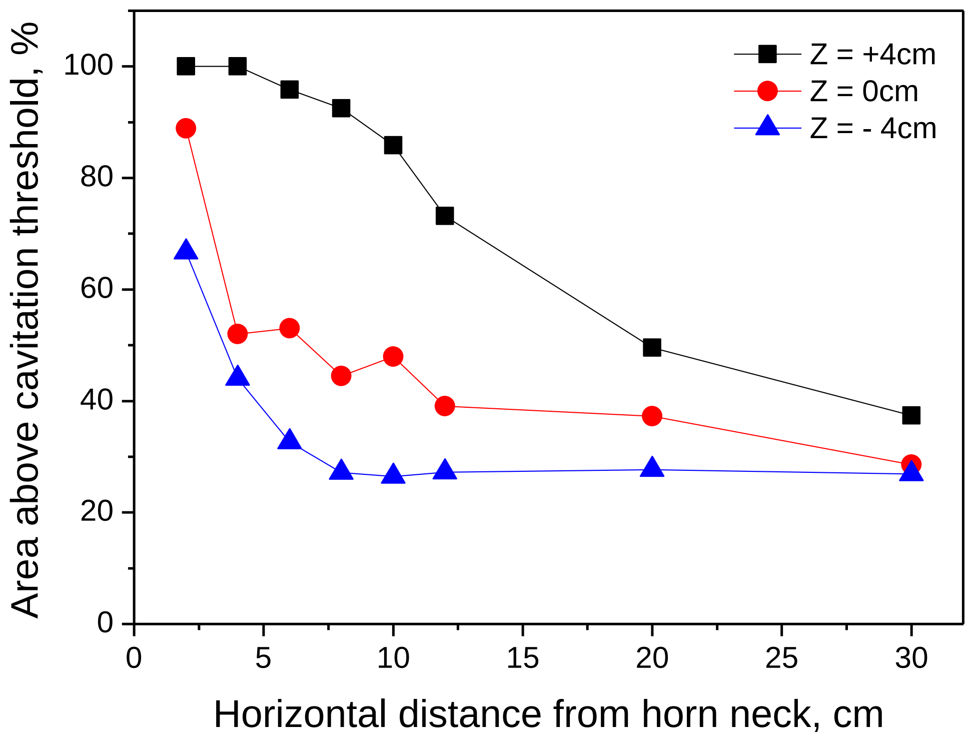


**Fig. 6.** Percentage of cavitation zones in different X-Y planes (% of cavitation zones = Measurements not less than 0.63 V in a X-Y plane / Total measurements in the X-Y plane × 100%; 0.63 V is measured cavitation threshold using acoustic emission method)

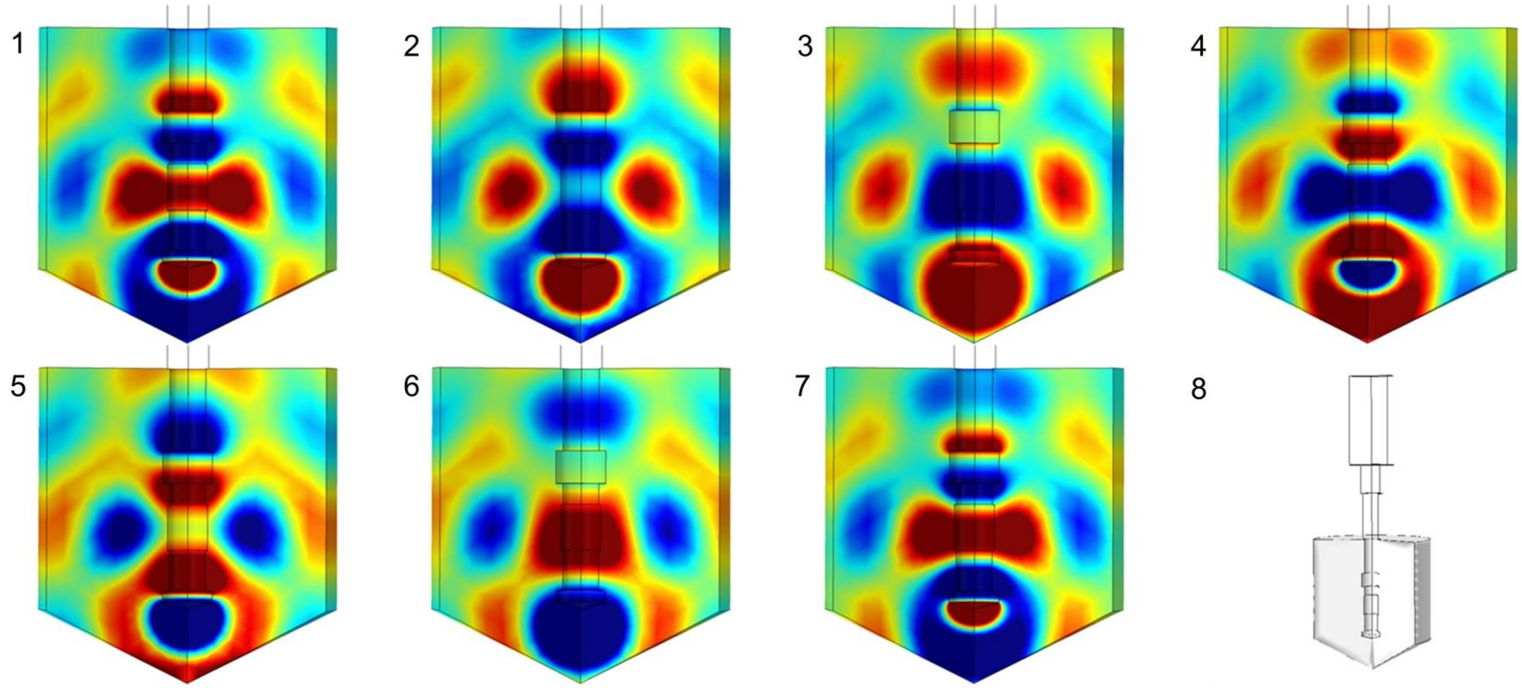


**Fig. 7.** Simulation of acoustic pressure propagation in proposed reactor configuration (red — up to + $1.59 \times 10^5$ Pa; blue color — down to – $1.59 \times 10^5$ Pa)

**Figure Captions**

**Fig. 1.** Simulation of acoustic pressure distribution in X-Z plane (Units for color labels and axes are Pa and mm, respectively)

**Fig. 2.** Simulation of acoustic pressure distribution in X-Y planes at different depths (1 — X-Y plane near water surface; 2 — X-Y plane in the middle of horn neck; 3 — X-Y plane at Z = 0 cm; 4-6 — X-Y planes at Z < 0 cm; units for color labels and axes are Pa and mm, respectively)

**Fig. 3.** Acoustic pressure distribution in Z-direction at different distances (2 cm, 5 cm and 10 cm) and power levels (50%, 75% and 100%; red dotted line is the cavitation threshold value of 0.63 V)

**Fig. 4.** 3D (left) and contour (right) mapping of hydrophone measurements in plexiglass tank (This scan was carried out at room temperature with 50% power input from power supply to transducer; a — X-Y plane at Z = +4 cm; b — X-Y plane at Z = 0 cm; c — X-Y plane at Z = –4 cm)

**Fig. 5.** Ultrasonic waveforms (left) and frequency spectra (right) observed in water at different power intensities (Convex feature in the waveform results from the sum of waveforms in different frequencies to the original waveform; units for magnitude of frequency spectra are arbitrary)

**Fig. 6.** Percentage of cavitation zones in different X-Y planes (% of cavitation zones = Measurements not less than 0.63 V in a X-Y plane / Total measurements in the X-Y plane × 100%; 0.63 V is measured cavitation threshold using acoustic emission method)

**Fig. 7.** Simulation of acoustic pressure propagation in proposed reactor configuration (red — up to + 1.59 × $10^5$ Pa; blue color — down to – 1.59 × $10^5$ Pa)